This is a repository copy of *Reactive spark plasma synthesis of CaZrTi2O7 zirconolite ceramics for plutonium disposition*.

White Rose Research Online URL for this paper:
http://eprints.whiterose.ac.uk/125886/

Version: Published Version

Reactive spark plasma synthesis of CaZrTi$_2$O$_7$ zirconolite ceramics for plutonium disposition

Shi-Kuan Sun, Martin C. Stennett, Claire L. Corkhill, Neil C. Hyatt[*]

Immobilisation Science Laboratory, Department of Materials Science and Engineering, University of Sheffield, Sheffield S1 3JD, United Kingdom

HIGHLIGHTS

- Rapid fabrication of zirconolite CaZr-Ti$_2$O$_7$ ceramics was demonstrated by reactive spark plasma sintering (RSPS).
- Zirconolite ceramics could be fully densified at a temperature as low as 1200 °C in 1h.
- Ceramics were formed with a controlled mean grain size of 1.88 ± 0.55 μm.

GRAPHICAL ABSTRACT
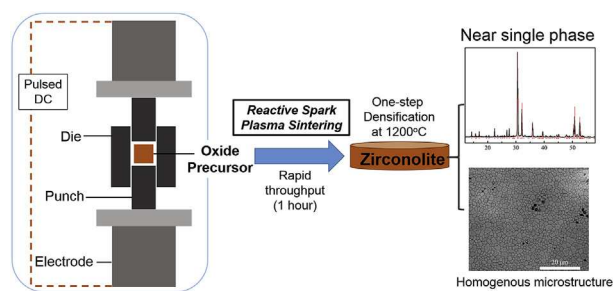
ARTICLE INFO

ABSTRACT

Near single phase zirconolite ceramics, prototypically CaZrTi$_2$O$_7$, were fabricated by reactive spark plasma sintering (RSPS), from commercially available CaTiO$_3$, ZrO$_2$ and TiO$_2$ reagents, after processing at 1200 °C for only 1 h. Ceramics were of theoretical density and formed with a controlled mean grain size of 1.9 ± 0.6 μm. The reducing conditions of RSPS afforded the presence of paramagnetic Ti^{3+}, as demonstrated by EPR spectroscopy. Overall, this study demonstrates the potential for RSPS to be a disruptive technology for disposition of surplus separated plutonium stockpiles in ceramic wasteforms, given its inherent advantage of near net shape products and rapid throughput.

Zirconolite, prototypically CaZrTi$_2$O$_7$, is proposed as an actinide host, for disposal of high level waste from nuclear fuel recycle, as a component of the Synroc composite ceramic, and as a tailored ceramic wasteform for excess civil and military plutonium [1–5]. For this purpose, synthetic and mineral zirconolites demonstrate the requisite stoichiometric flexibility, chemical durability, radiation tolerance, and long term stability in open geochemical environments [5,6].

The fabrication of zirconolite ceramics has been typically achieved by solid state synthesis, with a requirement for sintering at high temperature, typically 1400–1450 °C [7]; sintering at 1200 °C, has been shown to yield porous specimens [8]. Zirconolite ceramics of near theoretical density may be produced by hot isostatic pressing (HIPing) at ca. 1250 °C, but with a requirement for containment in a canister e.g. of stainless steel [9].

Fabrication times for ceramic wasteforms produced by conventional sintering and HIPing are typically several hours. In contrast, spark plasma sintering (SPS) is a rapid method for consolidation of ceramics of refractory materials, including UO$_2$, UN, and UC nuclear fuels [10–12]. In SPS, the material to be sintered

* Corresponding author.
    E-mail address: n.c.hyatt@sheffield.ac.uk (N.C. Hyatt).

is subject to uniaxial pressure, typically within a graphite die, and rapid heating by application of pulsed electric current; the associated electric field may also assist sintering [13—15]. SPS is potentially advantageous for production of ceramic wasteforms since it achieves rapid consolidation of ceramic bodies at lower temperature, potentially reducing the volatilisation of radionuclides, compared to conventional sintering. However, this application of SPS was only recently demonstrated, although in a diversity of examples, including: $CaZr_{1-x}Ce_xTi_2O_7$ zirconolite [16]; $Ln_2(Ti,Zr)_2O_7$ pyrochlores [17—21]; hollandite-rich ceramics [22]; $CaTh(PO_4)_2$, [23]; iodoapatites, [24—26]; and glass-composites [27].

Here, we demonstrate application of SPS to the rapid fabrication of high quality $CaZrTi_2O_7$ ceramics, from commercially available mixed metal oxides, as micron sized powders. Since the target ceramic is produced in a single step, with solid state reaction of reagents and sintering of the product phase occurring in parallel, we refer to this approach as *Reactive* Spark Plasma Sintering (RSPS). We distinguish this from *consolidation* of pre-synthesised powders employed in conventional SPS, as was generally applied in the examples above, including zirconolite ceramics [16]. In contrast, the RSPS approach has not been widely exploited and confined to relatively few examples, such as $Pb_{10}(VO_4)_{4.8}(PO_4)_{1.2}I_2$, $Gd_2Zr_2O_7$, and $Lu_2Ti_2O_7$ [19,21,24].

The raw materials used were $CaTiO_3$ (99%, ~325 mesh; Alfa Aesar), ZrO_2 (99%, 5 μm, Aldrich) TiO_2 — anatase (≥99%, ~325 Mesh; Aldrich). $CaTiO_3$, ZrO_2 and TiO_2 with a mole ratio of 1:1.025:1 were mixed by planetary milling for 20 min using zirconia media and isopropanol as a carrier fluid. The slurry was then dried overnight at 85 °C. An excess of ZrO_2 was utilised, relative to the ideal stoichiometric composition, since, in our experience, this results in near single phase materials.

Reactive Spark Plasma Sintering (RSPS) of zirconolite utilised 3 g of the oxide precursors, loaded into a cylindrical graphite die (diameter 20 mm), with thin graphite foil spacers to obtain a more uniform current flow. An HP-D 1050 SPS system (FCT Systeme GmBH) was used to process materials; samples were ramped to 900—1200 °C, at 50 °C/min followed by a dwell time, under uniaxial pressure of 15 MPa or 50 MPa. The reaction/sintering time was 10 min or 30 min; samples were cooled to room temperature at natural rate. The graphite foil and surface contamination was removed by light grinding with SiC paper.

Solid state synthesis of zirconolite was investigated by reaction sintering of oxide precursors at 900—1300 °C for 10 h under Ar gas (100 ml/min). Conventional sintering of zirconolite powder (from solid state reaction at 1300 °C) was achieved by forming green pellets of 20 mm × 10 mm (diameter × height) under uniaxial pressure of 50 MPa; these were sintered at 1450 °C for 10 h in air. All such processing used a ramp rate of 5 °C/min from/to room temperature.

Microstructures were observed using scanning electron microscopy (SEM; Inspect F50, FEI) on fracture or polished surfaces with a thermal etch (0.25 μm finish using SiC and diamond polishing media; thermal etch at 1100 °C for 1 h in air). Grain size determinations were made on >500 grains, using semiautomatic image analysis to calculate equivalent spherical diameters. The *Span* was calculated by $Span = (d_{0.9} - d_{0.1})/d_{0.5}$ to represent the width of grain size distribution. The bulk density of ceramics was determined using Archimedes' method by immersion in water. The phase assemblage was determined by X-ray diffraction (XRD; D2 Phaser, Bruker; Cu-Kα radiation, Ni-filter). Rietveld quantitative phase analysis (QPA) of XRD data was performed using the GSAS software package [28]. Electron Paramagnetic Resonance (EPR) measurements were carried out on a Bruker EMX-8/2.7 spectrometer operating in the X-band at 9.37 GHz and 1.7 mW, at 77 K; powder samples were contained in Spectrosil tubes.

The XRD patterns for the products after RSPS at various temperatures with a dwell time of 10 min, are shown in Fig. 1. In comparison with the starting materials (Fig. S1 in Supporting Information), no obvious changes could be seen in the product after heat treatment at 900 °C. For the product heat-treated at 1000 °C and 1100 °C, characteristic (221)/(40$\overline{2}$) and (004) reflections of $CaZrTi_2O_7$ (2M phase; $C2/c$) were apparent at $2\theta = 30.5°$ and 32.0°, respectively. The relative intensity of these reflections increased with increasing temperature, indicating increased yield of zirconolite, however, substantial unreacted $CaTiO_3$, TiO_2, and ZrO_2 remained. Near single phase zirconolite was obtained after heat treatment at 1200 °C, with trace residual $CaTiO_3$ and ZrO_2. No other ternary oxides could be identified after reaction at any temperature. The XRD patterns from the powdered bulk material and polished ceramic surface, after removal of the graphite foil, showed no significant difference (Fig. 1d and e, respectively).

For comparison, the solid state synthesis of zirconolite was investigated under argon atmosphere. The phase assemblage, as a function of reaction temperature, was very similar to that to RSPS (compare Fig. S2). In particular, near single phase zirconolite was only obtained at 1200 °C or 1300 °C, and was observed to be in equilibrium with $CaTiO_3$, TiO_2 and ZrO_2 at lower temperature; no other ternary oxides were identified. These results are consistent with the phase diagram of the CaO-ZrO_2-TiO_2 system in air [29] and suggest that the mechanism of the conventional solid state and RSPS reactions are identical. However, inspection of relative reflection intensities in the XRD patterns, showed that the zirconolite yield is reduced at lower processing temperatures in RSPS, compared to solid state synthesis, due to the short processing time and kinetic limitations.

SEM observations (backscattered electron images) of the fracture surface of RSPS zirconolite ceramics processed at 1100 °C and 1200 °C at 15 MPa, are shown in Fig. S3 and Fig. S4. Comparison of these microstructures revealed considerable porosity, observed as black contrast, in the sample processed at 1100 °C, which was all but eliminated after processing at 1200 °C. In these microstructures, the zirconolite phase appeared as mid grey contrast with residual ZrO_2 evident as bright contrast (consistent with XRD and
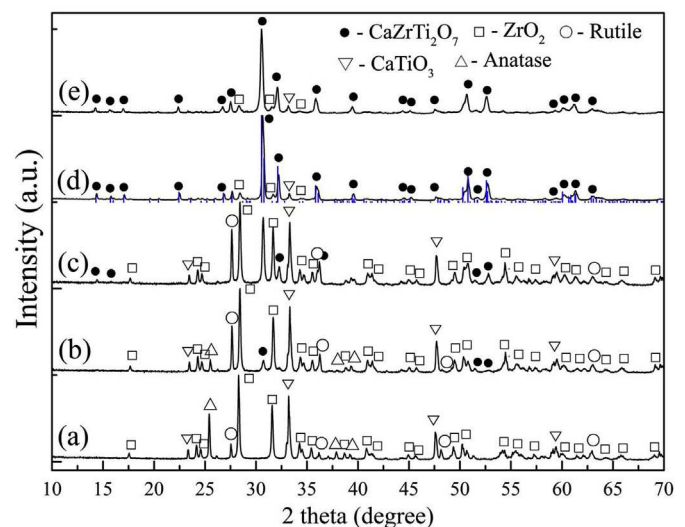
Fig. 1. XRD patterns of the products of RSPS at 900 °C (a), 1000 °C (b), 1100 °C (c), 1200 °C (d and e); patterns (a)-(d) were acquired from bulk powder specimens, whereas (e) was acquired from a polished ceramic surface; vertical blue lines are the reference diffraction pattern for zirconolite from Ref. [4]. (For interpretation of the references to colour in this figure legend, the reader is referred to the Web version of this article.)

confirmed by EDX, see Fig. S4). It was not possible to reliably identify the minor $CaTiO_3$ phase, since the backscattered electron coefficient ($\eta = 0.2772$) was similar to that of the major $CaZrTi_2O_7$ phase ($\eta = 0.2388$), as estimated using well established formulations [30]. Such a difference in relative contrast of ca. 3%, is acknowledged to make differentiation challenging in backscattered electron imaging [30].

Increasing uniaxial pressure from 15 MPa to 50 MPa, did not improve the phase assemblage and microstructure obtained after RSPS at 1200 °C for 10 min (compare Fig. S4 and Fig. S5). Rietveld analysis of XRD data from this material afforded a quantitative phase assemblage of: $CaZrTi_2O_7 - 84.8(1)$ wt%, $CaTiO_3 - 8.4(4)$ wt%, and $ZrO_2 - 6.8(4)$ wt%. However, increasing the dwell time to 30 min at 1200 °C, under 15 MPa, further improved the yield of zirconolite, as assessed from both XRD data and SEM observations. Rietveld analysis of XRD data, Fig. 2a, afforded a quantitative phase assemblage of: $CaZrTi_2O_7 - 97.0(1)$ wt%, $CaTiO_3 - 2.1(2)$ wt%, and $ZrO_2 - 0.9(1)$ wt%. Consistent with this analysis, SEM observation of the ceramic microstructure, as both a fracture and polished surface (Fig. 2b and c), together with EDX analysis (Fig. S6), revealed no obvious accessory phases, due to their low concentration (and negligible difference in contrast of $CaTiO_3$ and $CaZrTi_2O_7$). The microstructure of the polished ceramic surface (after thermal etch of 1 h at 1100 °C in Ar) demonstrated a homogenous and equiaxed grain structure, and absence of observable porosity (the isolated, angular, dark contrast is due to grain pull out during polishing). The mean grain size was $1.9 \pm 0.6\,\mu m$ with a *span* of 0.80, and the density was determined to be 4.41(3) g cm^{-3}, identical to the theoretical density of 4.40 g cm^{-3}. In contrast, the microstructure of zirconolite ceramic produced by conventional sintering at 1450 °C,

exhibited some noticeable porosity at grain triple points and a larger mean grain size of $15.9 \pm 7.2\,\mu m$ with *span* of 1.34, as shown in Fig. S7. No further improvement in phase assemblage by RSPS was attained by increasing the reaction temperature to 1300 °C.

The reducing atmosphere imposed by the graphite die and vacuum applied in RSPS could be expected to reduce Ti^{4+} to Ti^{3+} in zirconolite. Indeed, materials produced by RSPS were black in colour when ground to a fine powder, typical of Magnelli phases, Ti_nO_{2n-1}, which contain considerable of Ti^{3+}. Thus, Electron Paramagnetic Resonance (EPR) spectroscopy was applied to zirconolite powder specimens (at 77 K) to ascertain the presence of Ti^{3+} species. The EPR spectrum of RSPS zirconolite (1200 °C, 30 min, 15 MPa; see Fig. S8) demonstrated the presence of a strong resonance centred at $g \approx 1.94$, which was also observed in the EPR spectra of zirconolite prepared by solid state synthesis under Ar (1300 °C, 10 h) and annealed under 5% H_2/N_2 (1200 °C, 10 h). This signal was observed by Begg et al. [31], in the EPR spectrum (at 80 K) of zirconolite reduced under flowing 3.5% H_2/N_2 (1200 °C, 12 h) and attributed to paramagnetic Ti^{3+} species, verified by Ti K-edge XANES. Thus, we infer the presence of reduced Ti^{3+} in the ceramics prepared by RSPS and under Ar or 5% H_2/N_2 in this study, presumably accommodated within the zirconolite phase, charge compensated by oxygen vacancies in accordance with the study of Begg et al. The EPR spectra of the zirconolites prepared under Ar and 5% H_2/N_2 in this study also exhibit additional features, the origin of which is not known, but which implies a subtle difference in the precise defect chemistry.

Reactive Spark Plasma Sintering has been shown to yield zirconolite ceramics of theoretical density from commercially available reagents, at 1200 °C and 15 MPa, with a process time of only
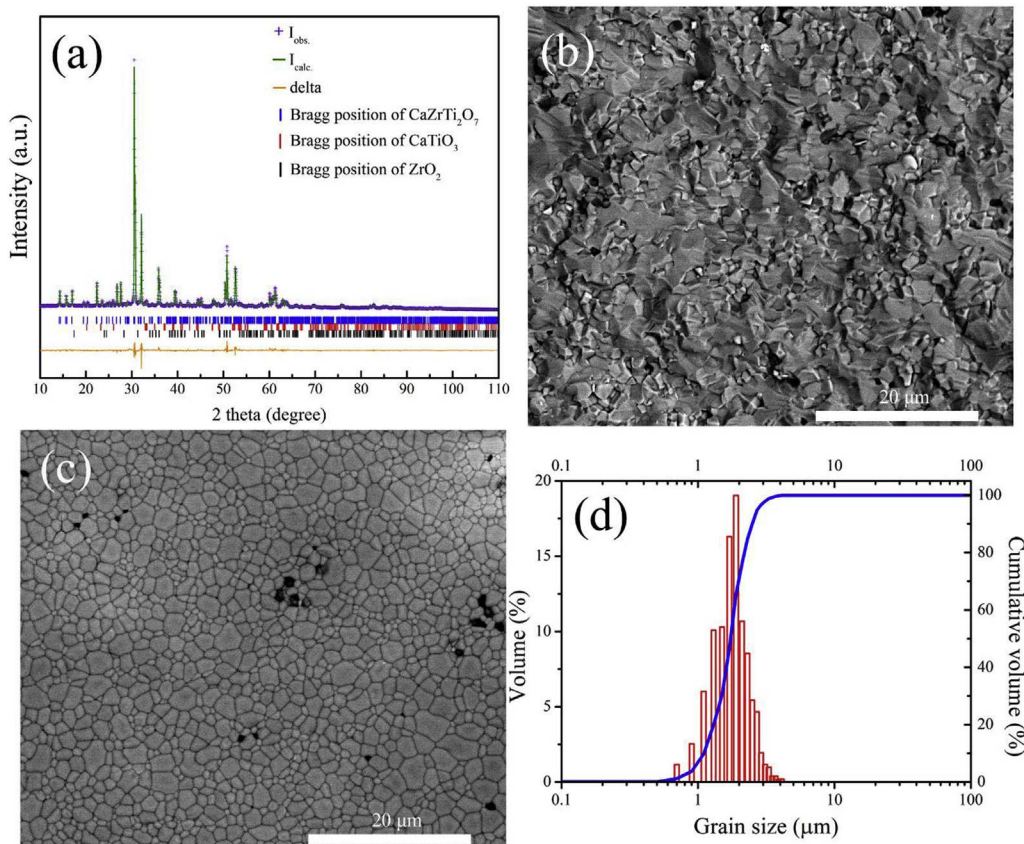

Fig. 2. RSPS of zirconolite at 1200 °C, 15 MPa, for 30min; a) Rietveld fit of XRD data for QPA, with $R_p = 8.23\%$, $R_{wp} = 6.08\%$ and $\chi^2 = 3.24$; (b) and (c) SEM observation of polished and fracture surface specimens, respectively; (d) Grain size distribution.

1 h. The resulting ceramics are characterised by partial reduction of Ti^{4+} to Ti^{3+} and possibly cation/vacancy disorder. Formation of the zirconolite phase, and sintering, progressed in tandem, with no evidence of a mechanism different from solid state reaction.

RSPS could be a disruptive technology for nation states, such as the UK, currently considering the disposition of surplus separated plutonium stockpiles in ceramic wasteforms. The rapid process time achievable in RSPS would translate to high material throughput, if the technology could be deployed at the desired scale. The batch wise nature of the RSPS process would be advantageous for criticality, accountancy and safeguards controls. Consolidation is near net shape in SPS, such that ceramics could conceivably be fabricated with requisite dimensions to fit within current standard PuO_2 storage cans, compatible with existing stores. The use of a graphite die may not be desirable for processing of fissile materials, given its moderating characteristics; however, a recent review highlighted the use of a wide range of advanced alloys and ceramics as die materials [15], including boron nitride, which would be advantageous given the high neutron absorption cross section of boron. The potential reduction of Pu^{4+} to Pu^{3+} under RSPS conditions could stabilise a Pu^{3+} perovskite accessory phase, which would not be desirable given the lower radiation tolerance of this structure. Indeed, stabilisation of a Ce^{3+} perovskite phase was observed in a recently published study of Ce-zirconolite consolidation by SPS utilising a graphite die [16]. This could be mitigated by use of a boron nitride die, tuning of the zirconolite composition and charge compensation mechanisms, or alternative choice of ceramic wasteform. Industrial scale automated SPS systems have been operated commercially for fabrication of large scale components [15,32,33], and small scale systems have operated with radiological materials [10—12,23]. Further investigation of the application of SPS to the fabrication of ceramic waste forms, particularly for disposition of surplus plutonium, and maturation and adaptation of the technology for nuclear applications, would be desirable.

Acknowledgements

Appendix A. Supplementary data

Supplementary data related to this article can be found at https://doi.org/10.1016/j.jnucmat.2017.12.021.

References

[1] H.J. Rossell, Nature 283 (1980) 282.
[2] R.C. Ewing, W.J. Weber, J. Lian, J. Appl. Phys. 95 (2004) 5949.
[3] W.E. Lee, M.I. Ojovan, M.C. Stennett, N.C. Hyatt, Adv. Anal. Chem. 105 (2006) 3.
[4] K.R. Whittle, N.C. Hyatt, K.L. Smith, I. Margiolaki, F.J. Berry, K.S. Knight, G.R. Lumpkin, Am. Mineral. 97 (2012) 291.
[5] G.R. Lumpkin, Elements 2 (2007) 365.
[6] G.R. Lumpkin, K.L. Smith, R. Gieré, C.T. Williams, Geological Society, London 236 (2004) 89. Special Publications.
[7] D.P. Reid, M.C. Stennett, B. Ravel, J.C. Woicik, N. Peng, E.R. Maddrell, N.C. Hyatt, Nucl. Instrum. Methods Phys. Res. Sect. B Beam Interact. Mater. Atoms 268 (2010) 1847.
[8] G.J. Wen, K.B. Zhang, D. Yin, H.B. Zhang, J. Nucl. Mater. 466 (2015) 113.
[9] J. Squire, E.R. Maddrell, N.C. Hyatt, M.C. Stennett, Int. J. Appl. Ceram. Technol. 12 (2015) E92.
[10] H. Muta, K. Kurosaki, M. Uno, S. Yamanaka, J. Mater. Sci. 43 (2008) 6429.
[11] L.H. Ge, G. Subhash, R.H. Baney, J.S. Tulenko, E. McKenna, J. Nucl. Mater. 435 (2013) 1.
[12] D. Salvato, J.F. Vigier, M. Cologna, L. Luzzi, J. Somers, V. Tyrpekl, Ceram. Int. 43 (2017) 866.
[13] Z.A. Munir, U. Anselmi-Tamburini, M. Ohyanagi, J. Mater. Sci. 41 (2006) 763.
[14] S. Grasso, Y. Sakka, G. Maizza, Sci. Technol. Adv. Mater. 10 (2009) 053001.
[15] O. Guillon, J. Gonzalez-Julian, B. Dargatz, T. Kessel, G. Schierning, J. Rathel, M. Herrmann, Adv. Eng. Mater. 16 (2014) 830.
[16] B.M. Clark, S.K. Sundaram, S.T. Misture, Sci. Rep. 7 (2017) 5920.
[17] R. Kumar, K. Singh, D. Chakravarty, A. Chowdhury, Scripta Mater. 117 (2016) 37.
[18] J. Wen, C. Sun, P.P. Dholabhai, Y. Xia, M. Tang, D. Chen, D.Y. Yang, Y.H. Li, B.P. Uberuaga, Y.Q. Wang, Acta Mater. 110 (2016) 175.
[19] L. Wang, X.Y. Shu, X.R. Lu, Y.L. Wu, Y. Ding, S. Zhang, Mater. Lett. 196 (2017) 403.
[20] P.K. Kulriya, T.K. Yao, S.M. Scott, S. Nanda, J. Lian, J. Nucl. Mater. 487 (2017) 373.
[21] L. An, A. Ito, T. Goto, J. Am. Ceram. Soc. 94 (2011) 3851.
[22] P. Tumurugoti, B.M. Clark, D.J. Edwards, J. Amoroso, S.K. Sundaram, J. Solid State Chem. 246 (2017) 107.
[23] K. Popa, M. Cologna, L. Martel, D. Staicu, A. Cambriani, M. Ernstberger, P.E. Raison, J. Somers, J. Eur. Ceram. Soc. 36 (2016) 4115.
[24] S. Le Gallet, L. Campayo, E. Courtois, S. Hoffmann, Y. Grin, F. Bernard, F. Bart, J. Nucl. Mater. 400 (2010) 251.
[25] T.K. Yao, F.Y. Lu, H.T. Sun, J.W. Wang, R.C. Ewing, J. Lian, J. Am. Ceram. Soc. 97 (2014) 2409.
[26] A. Coulon, D. Laurencin, A. Grandjean, S. Le Gallet, L. Minier, S. Rossignol, L. Campayo, J. Eur. Ceram. Soc. 36 (2016) 2009.
[27] J.W. Lloyd, M.C. Stennett, R.J. Hand, J. Nucl. Mater. 469 (2016) 51.
[28] B.H. Toby, J. Appl. Crystallogr. 34 (2001) 210.
[29] D. Swenson, T.G. Nieh, J.H. Fournelle, J. Am. Ceram. Soc. 81 (1998) 3249.
[30] I. J, D.E. Newbury, P. Echlin, D.C. Joy, A.D. Romig Jr., C.E. Lyman, C. Fiori, E. Lifshin, Scanning Electron Microscopy and X-Ray Microanalysis, second ed., Plenum Press, New and London, 2012.
[31] B.D. Begg, E.R. Vance, B.A. Hunter, J.V. Hanna, J. Mater. Res. 13 (1998) 3181.
[32] M. Tokita, Mater. Sci. Forum (1999) 83, 308-311.
[33] M. Tokita, Mater. Sci. Forum (2003) 39, 423-425.